Determination of the Orientation of the Magnetic Axes of the Cyano-MetMb Complexes of Point Mutants of Myoglobin by Solution ^{1}H NMR: Influence of His E7 → Gly and Arg CD3 → Gly Substitutions

Krishnakumar Rajarathnam,[†] Gerd N. La Mar,*[,†] Mark L. Chiu,[‡] and Stephen G. Sligar[‡]

Contribution from the Department of Chemistry, University of California, Davis, California 95616, and Department of Biochemistry, Physiology and Biophysics and The Beckman Institute for Advanced Science and Technology, University of Illinois, Urbana, Illinois 61801. *Received March 5, 1992*

Abstract: A method is described for obtaining the axes of the diagonal paramagnetic susceptibility tensor for the low-spin cyanide complexes of distal point mutants of ferric sperm whale myoglobin (metMbCN). It relies on using the crystal coordinates of the wild-type (WT) protein for that portion of the molecule unperturbed by the point mutation, together with the experimental dipolar shifts, to search for the Euler rotation that correctly converts the crystal coordinates to the magnetic axes. The complete set of ^{1}H NMR dipolar shifts is shown to lead to the determination of the magnetic anisotropies as well as the orientation of the magnetic axes for WT metMbCN. Various sets of input ^{1}H NMR dipolar shifts for protons not only emphasizing the proximal side of the heme but also considering distal backbone protons and the structurally conserved Phe CD1 are shown to lead to well-defined magnetic axes for WT metMbCN with closely clustered Euler angles. The tilt of the major magnetic axis from the heme normal, the projection of this tilt on the heme plane, and the position of the rhombic axies projected on the heme plane range only over 1.5°, ~10°, and ~10°, respectively, for nine different data sets comprising as many as 37 to as few as five input dipolar shifts. The ^{1}H NMR spectra of the metMbCN complexes of a strongly perturbed (His E7 → Gly) and a minimally perturbed (Arg CD3 → Gly) point mutant are analyzed to yield the assignments necessary to define the magnetic axes. Using a variety of input data sets of dipolar shifts limited to the residues expected to be unperturbed by distal point mutation, the magnetic axes were determined by a three parameter least-square search for both the His E7 → Gly and Arg CD3 → Gly mutants. For the E7 Gly mutant, the major magnetic axis tilt is minimally altered, but the projection of the tilt is rotated by ~45°; the CD3 Gly mutant yields a magnetic axes orientation within the range defined by different data sets of WT metMbCN. However, simulation of the predicted dipolar shift based on systematic changes is used to show that the axes of the CD3 Gly mutant differ from those of the WT by a very small (2°) rotation of the projection of the tilt of the major axis, rather than from a change in tilt. Inasmuch as the orientation of the magnetic axes can be related to distal steric tilt of the isostructural Fe-CO unit in WT MbCO, the present demonstration that magnetic axes can be determined for point mutants has significant implications for the elucidation of steric constraints on bound ligands in a variety of low-spin hemoproteins.

Introduction

The intrinsically high information content of the hyperfine shifts of paramagnetic hemoproteins in general, and low-spin ferric systems in particular, has been recognized for a long time.[1,2] The advantageous properties that enhance the interest in low-spin ferric heme systems are as follows: an exceedingly short electron spin relaxation time which results in narrow ^{1}H NMR lines, the presence of a single unpaired electron spin in a d_π orbital, which allows a quantitative interpretation of the delocalized spin density, and the presence of substantial magnetic anisotropy that imposes significant dipolar shifts to residues in the active site.[2] This latter property is particularly valuable in that it allows the use of the iron paramagnetism to probe the geometry of nonbonded residues. This dipolar shift, δ_{dip}, is given by the general relation:[3,4]

$$\delta_{dip} = \frac{-1}{3N}\left[\Delta\chi_{ax}F_{ax}(\theta,\varphi,r) + \frac{3}{2}\Delta\chi_{rh}F_{rh}(\theta,\varphi,r)\right] \quad (1)$$

with the anisotropies:

$$\Delta\chi_{ax} = \chi_{zz} - \frac{1}{2}(\chi_{xx} + \chi_{yy}),\ \Delta\chi_{rh} = \chi_{xx} - \chi_{yy} \quad (2)$$

and geometric factors:

$$F_{ax} = (3\cos^2\theta - 1)r^{-3} \text{ and } F_{rh} = \sin^2\theta\cos 2\varphi\, r^{-3} \quad (3)$$

with θ and φ as the polar and azimuthal angles in the magnetic coordinate system in which the susceptibility tensor, χ, (with components χ_{zz}, χ_{xx}, χ_{yy}) is diagonal; this coordinate system is generally not known. However, if an abritrary metal-centered coordinate system, r, θ', φ', such as that derived from an X-ray structure, is available, eq 1 can be recast to:[5,6]

$$\delta_{dip} = \frac{-1}{3N}\left[\Delta\chi_{ax}F'_{ax}(\theta',\varphi',r) + \frac{3}{2}\Delta\chi_{rh}F'_{rh}(\theta',\varphi',r')\right]\mathbf{R}(\alpha,\beta,\gamma) \quad (4)$$

where F'_{ax} and F'_{rh} are the same geometric factors expressed in the metal-centered coordinate system and $\mathbf{R}(\alpha,\beta,\gamma)$ is the Euler rotation matrix[7] that rotates the X-ray derived coordinates system

* Address correspondence to this author.
[†] Univeristy of California.
[‡] University of Illinois.

(1) Wüthrich, K. *Struct. Bonding (Berlin)* **1970**, *8*, 53-121. Morrow, J. S.; Gurd, F. R. N. *CRC Crit. Rev. Biochem.* **1975**, *3*, 221-287. La Mar, G. N.; Walker, F. A. In *The Porphyrins*; Dolphin, D., Ed.; Academic Press: New York, NY, 1978; Vol. IVB, pp 61-159. Keller, R. M.; Wüthrich, K. In *Biological Magnetic Resonance*; Berliner, L. J.; Reuben, J., Eds.; Plenum Press: New York, NY, 1980; Vol. 3, pp 1-52. La Mar, G. N. In *Biological Application of Magnetic Resonance*; Shulman, R. G., Ed.; Academic Press: New York, 1979; pp 305-343. Satterlee, J. D. *Annu. Rev. NMR Spectrosc.* **1985**, *17*, 80-178.
(2) Shulman, R. G.; Glarum, S. H.; Karplus, M. *J. Mol. Biol.* **1971**, *57*, 93-115.
(3) Jesson, J. P. In *NMR of Paramagnetic Molecules*; La Mar, G. N., Horrocks, W. D., Jr., Holm, R. H., Eds.; Academic Press: New York, NY, 1973; pp 1-52.
(4) Bertini, I.; Luchinat, C. In *Paramagnetic Molecules in Biological Systems*; Benjamin/Cummings Publication Co., Inc.: Menlo Park, CA, 1986; pp 19-46.
(5) Emerson, S. D.; La Mar, G. N. *Biochemistry* **1990**, *29*, 1556-1566.
(6) Williams, G.; Clayden, N. J.; Moore, G. R.; Williams, R. J. P. *J. Mol. Biol.* **1985**, *183*, 447-460. Feng, Y.; Roder, H.; Englander, S. W. *Biochemistry* **1990**, *29*, 3494-3504. Gao, Y.; Boyd, J.; Pielak, G. J.; Williams, R. J. P. *Biochemistry* **1991**, *30*, 1928-1934.
(7) Arfkin, G. In *Mathematical Methods for Physicists*; Academic Press: Orlando, FL, 1985; pp 199-200.

0002-7863/92/1514-9048$03.00/0

(r,θ',φ') into the magnetic coordinate system (r,θ,φ).

The quantitative use of δ_{dip} for any resonance requires the availability of the appropriate X-ray coordinates, the magnetic anisotropy, and the Euler rotation matrix. The magnetic anisotropies ($\Delta\chi_{ax}$ and $\Delta\chi_{rh}$) reflect on the nature of the ligand field and electronic structure of the iron;[8] the geometric factors (F_{ax} and F_{rh}) yield information on the orientation of residues that define the molecular structure of the active site; and the orientation of the susceptibility tensor ($\mathbf{R}(\alpha,\beta,\gamma)$) yields information on the deformation of the pseudo-4-fold symmetry of the free heme[9] upon placement in the asymmetric protein pocket.[5,6] X-ray coordinates for numerous low-spin ferric hemoproteins have been available for sometime,[10-12] as have been the theoretical estimates of the components of the susceptibility tensor based[8] on the low-temperature **g** tensor.[13] The major reason that quantitative interpretation of dipolar shifts has not been realized earlier is lack of information on the rotation matrix and the dipolar shifts in eq 2. Recent advances in the direct applicability of modern 1D and 2D NMR methods to paramagnetic proteins,[14,15] however, have provided the methods for obtaining the unambiguous assignments that can yield δ_{dip} for the majority of active site residues including those closest to the iron. The orientation of the magnetic axes in both ferricytochrome[6] and the cyanide complex of ferric myoglobin,[5] metMbCN, have been determined recently based on a least-square search of $\mathbf{R}(a,\beta,\gamma)$ that correctly predicts all δ_{dip}.

For the particular case of interest here, wild-type (WT) sperm whale metMbCN, NMR analysis has revealed[5] that the major magnetic axis is tilted from the heme normal in a manner very similar to the Fe–CO tilt in the isostructural MbCO complex.[11] This ligand tilt and, by direct inference, the tilt of the magnetic axis with the Fe–CN unit have been directly attributed to distal residues (sepcifically the invariant E7 His) in sterically destabilizing the bound CO in order to favor O_2 binding in the native protein.[16] The Fe^{+2}–CO and Fe^{+3}–CN groups are isostructural, and in the one protein where X-ray structures have been solved for both forms,[17] a similar tilt of the bonding axis is observed. In low-spin ferric cyanide model complexes, the major magnetic axis is invariably normal to the heme.[9] It has been proposed[5] that the orientation of the major magnetic axis in metMbCN serves as a direct measure of the degree of Fe–CN tilt and hence is a measure of the distal steric interactions. Since crystal structures have not been reported for the particular mutants of interest and generally will not be practical for the range of mutants that will become available, a strategy must be deveoped and tested for determining the magnetic axes based on the WT crystal coordinates.[11]

In this report we consider the necessary information and analyze an accessible methodology for determining the magnetic axes of a general distal point mutant of sperm whale metMbCN. Thereafter, we assign the necessary resonances in two specific point mutants to explore the interpretiation of the effects of major and minor distal perturbations on both the ability to determine magnetic axes and the nature of the changes in the orientation of the magnetic axes. An idealized scenario would have an ensemble of point mutants producing systematically peturbed ^1H NMR spectral parameters which can be quantitatively interpreted on the basis of changes in either the orientation of the axis or the anisotropies; at worst changes in both must be considered. In order to determine changes in anisotropies, we must first demonstrate that the NMR data are capable of experimentally yielding the magnetic anisotropies, as opposed to relying on the available theoretical values.

The two point mutants of sperm whale Mb[18] that are selected for study are His E7 → Gly and Arg CD3 → Gly. The former eliminates the putative (imidazole) side chain that has been proposed to be responsible for the axial ligand and magnetic z-axis tilt[16,19] and shows substantial changes in the NMR spectrum that must represent a major perturbation. The CO binding properties of the protein are also significantly perturbed.[20] The latter mutant replaces a residue involved in a salt bridge that holds the distal pocket closed;[11,22] the Arg side chain itself does not intrude into the ligand binding pocket, and hence minimal effects on the steric constraints on bound ligand are expected. Detailed functional studies of this mutant reveal inconsequential changes in CO binding.[21] We address herein the following questions for the WT protein: Can the magnetic anisotropies, as well as the orientation of the axes, be experimentally determined from the available NMR data? Which of the detailed structural elements of the WT protein can be retained for a point mutant for the purposes of determining the magnetic axes? How well are the magnetic axes defined for any given input NMR data set? For the mutants we pose the following questions: How well are the magnetic axes determined? Can the magnetic anisotropies be determined as well? How small a perturbation of the magnetic axes can be defined by the changes in NMR parameters? And lastly, do the His F8 ring protons serve as qualitative indicators of the degree of tilt of the magnetic z-axis as proposed previously?

Experimental Section

Sample Preparation. His E7 → Gly and Arg CD3 → Gly Mb mutants are obtained as reported by Springer and Sligar.[18] Cyanometmyoglobin complexes, metMbCN, are prepared by exchanging the oxidized protein on an Amicon ultrafiltration device with a solution of ^2H_2O containing 0.2 M KCl and 0.02 M KCN, pH 8.6.

^1H NMR Measurements. All ^1H NMR spectra were collected on either GE Ω 500 or Nicolet NT-500 spectrometers operating in the quadrature mode at 500 MHz. Steady-state 1D nuclear Overhauser effect difference spectra for the hyperfine shifted peaks were obtained over the temperature range 10–40 °C by irradiating the desired resonance for 150–200 ms with the decoupler and subtracting from this a similar spectrum with the decoupler well off-resonance. The difference spectra consist of 2000–2500 scans collected with a 400-ms recycle time. The WEFT[23] pulse sequence was used to produce spectra that suppress the slowly relaxing diamagnetic envelope and enhance the intensity of broad, rapidly relaxed signals.

The magnitude COSY, MCOSY (n-type), spectra[24] were collected at 20, 30, and 40 °C in ^2H_2O over a spectral window of 11 049 Hz (for E7 Gly mutant) using 1024 $t2$ complex points; 96 scans were collected for each block with a total of ~400–500 $t1$ blocks. The repetition time was 350 ms, and the total acquisition time is ~6–8 h. The residual ^1H_2O was saturated with a 200-ms decoupler pulse in the predelay time. Phase-sensitive 2D NOE (NOESY) spectra were collected at 30 °C in ^2H_2O over a spectral window of 25 000 Hz using 1024 complex points in the $t2$ dimension; 96 scans were collected for each of 238 $t1$ increments; quadrature detection along the $t1$ dimension was achieved using the TPPI method.[25] The mixing time used in this experiment was 50 ms. The

(8) Horrocks, W. D., Jr.; Greenberg, E. S. *Biochim. Biophys. Acta* **1973**, *322*, 38–44.
(9) Palmer, G. In *The Porphyrins*; Dolphin, D., Ed.; Academic Press: New York, NY, 1979; Vol. IV, pp 313–353. Byrn, M. P.; Katz, B. A.; Keder, N. L.; Levan, K. R.; Magurany, C. J.; Miller, K. M.; Pritt, J. W.; Strouse, C. E. *J. Am. Chem. Soc.* **1983**, *105*, 4916–4922. Inniss, D.; Soltis, S. M.; Strouse, C. E. *J. Am. Chem. Soc.* **1988**, *110*, 5644–5650.
(10) Takano, T. *J. Mol. Biol.* **1977**, *110*, 537–568, 569–588.
(11) Kuriyan, J.; Wilz, S.; Karplus, M.; Petsko, G. A. *J. Mol. Biol.* **1986**, *192*, 133–154.
(12) Takano, T.; Dickerson, R. E. *J. Mol. Biol.* **1981**, *153*, 78–94, 95–115.
(13) Hori, H. *Biochim. Biophys. Acta* **1971**, *251*, 227–235.
(14) Emerson, S. D.; La Mar, G. N. *Biochemistry* **1990**, *29*, 1545–1556.
(15) Yu, L. P.; La Mar, G. N.; Rajarathnam, K. *J. Am. Chem. Soc.* **1990**, *112*, 9527–9534.
(16) Phillips, S. E. V. *J. Mol. Biol.* **1980**, *142*, 531–554. Collman, J. P.; Brauman, J. I.; Halbert, T. R.; Suslick, K. *Proc. Natl. Acad. Sci. U.S.A.* **1976**, *73*, 3333–3337.
(17) Steigemann, R. W.; Weber, E. *J. Mol. Biol.* **1979**, *127*, 309–338.
(18) Springer, B. A.; Sligar, S. G. *Proc. Natl. Acad. Sci. U.S.A.* **1987**, *84*, 8961–8965.
(19) Stryer, L. *Biochemistry*, 3rd ed.; W. H. Freeman & Co.: New York, NY, 1988.
(20) Rohlfs, R. J.; Mathews, A. J.; Carver, T. E.; Olson, J. S.; Springer, B. A.; Egeberg, K. D.; Sligar, S. G. *J. Biol. Chem.* **1990**, *265*, 3168–3176.
(21) Carver, T. E.; Olson, J. S.; Smerdon, S. J.; Krzywda, S.; Wilkinson, A. J.; Gibson, Q. H.; Blackmore, R. S.; Dezz Ropp, J.; Sligar, S. G. *Biochemistry* **1991**, *30*, 4697–4705.
(22) Ringe, D.; Petsko, G. A.; Kerr, D. E.; Ortiz de Montellano, P. R. *Biochemistry* **1984**, *23*, 2–4.
(23) Gupta, R. K. *J. Magn. Reson.* **1976**, *24*, 461–465.
(24) Bax, A. *Two Dimensional Nuclear Magnetic Resonance in Liquids*; D. Reidell Publishing Company: Dordrecht, Holland, 1982.
(25) Marion, D.; Wüthrich, K. *Biochem. Biophys. Res. Commun.* **1983**, *113*, 967–974.

Table I. NMR Resonances Whose Dipolar Shifts Serve as Input Data for Magnetic Axes Determination[a]

		data set code								
		proximal and limited distal					proximal only			minimal
		A	B	B′	C	C′	D	D′	E	F
Proximal Side										
F helix	Leu F4 $C_\alpha H$	1	1	1	1	1	1	1	1	0
	Ala F5 $C_\alpha H$, $C_\beta H_3$	2	2	2	2	2	2	2	0	0
FG corner	His FG3 $C_\beta H$, $C_\beta H'$	2	2	0	2	0	2	0	0	0
	$C_\delta H$	1	1	1	1	1	1	1	1	1
	$C_\epsilon H$	1	1	1	1	1	1	1	1	0
	Ile FG5 $C_\alpha H$, $C_\beta H$, $C_\gamma H'$	3	3	3	3	3	3	3	3	0
	$C_\gamma H_3$, $C_\delta H_3$, $C_\gamma H$	3	3	3	3	3	3	3	3	3
G helix	Leu G5 $C_\gamma H$, $C_{\delta 2} H_3$	2	2	0	2	0	2	0	0	0
H helix	Phe H15 ring CHs	3	3	3	3	3	3	3	0	0
	Tyr H23 C_ϵHs	1	1	0	1	0	1	0	0	0
	total proximal input	19	19	14	19	14	19	14	9	4
distal side										
CD corner	Phe CD1 $C_\zeta H$	1	1	1	1	1	0	0	0	1
	C_ϵHs, C_δHs	2	2	2	2	2	0	0	0	0
E helix	backbone, C_αHs	3	3	3	0	0	0	0	0	0
other distal[b]		12	0	0	0	0	0	0	0	0
	total distal input	18	6	6	3	3	0	0	0	1
	total input	37	25	20	22	17	19	14	9	5

[a] The side chain residues are listed by their helical origin and the number of the described input data points listed under these various data sets. [b] This consists of the 12 signals from the side chains of Thr E10 (2), Ala E14 (1), aromatic rings of Phe B14 and CD4 (6), the methyls of Leu B10 (2), and $C_\gamma H_3$ of Ile G8 (1).

reptition time was 290 ms, and the total acqusition time was ~12 h. The residual ^1H_2O signal was irradiated for 200 ms with a decoupler pulse in the predelay time.

All 1D data were processed on a SPARC station using GE UNIX Ω software. All 2D data were processed on a Silicon Graphics Work Station using the Felix program written by Dr. Dennis Hare. The MCOSY data were processed using both an unshifted sinebell-square and an exponential (3-Hz line broadening) window function in both the $t2$ and the $t1$ dimensions. The data were processed using either 256, 512, or 1024 data points along the $t2$ dimension and using either 256 or all the points along the $t1$ dimension, and in all cases final data sets were zero-filled to 2048 × 2048 real points. The NOESY data were processed using a 30° shifted sinebell-square window in both dimensions. The window function was applied over 512 points along $t2$ and over all points the $t1$ dimension; all data sets were zero-filled to 2048 × 2048 points. All chemical shifts are referenced to 2,2-dimethyl-2-silapentane-5-sulfonate, DSS, through the residual solvent signal.

Magnetic Axes Determination. The observed dipolar shifts, δ_{dip}(obsd), are calculated using the following equation:

$$\delta_{obsd} = \delta_{hf} + \delta_{dia} \quad (5)$$

where δ_{obsd} is the observed shift in metMbCN referenced to DSS, δ_{dia} is the shift in the isostructural diamagnetic complex (such as MbCO),[26] and δ_{hf} is the hyperfine (paramagnetic) contribution to the shift. For protons whose chemical shifts in MbCO are not available, δ_{dia} is calculated using the equation:

$$\delta_{dia} = \delta_{tetra} + \delta_{rcs} \quad (6)$$

where δ_{tetra} is the tetrapeptide shift[27] and δ_{rcs} is the ring current shift due to the heme and aromatic side chains and is calculated using the eight loop model[28] and the X-ray coordinates of the MbCO complex.[11] The use of δ_{dia} for WT MbCO appears well justified. For the most part, such assignments for mutants are not available. Moreover, the very limited assignments for proximal residues in E7 Gly MbCO that are available indicate negligible differences <0.02 ppm, from WT MbCO. Hence the use of WT MbCO δ_{dia} appears very reasonable. δ_{hf} generally has two components,[1,5] $\delta_{hf} = \delta_{dip} + \delta_{con}$, where the dipolar shift is given by eq 4 and the contact shift reflects delocalized spin density. For noncoordinated amino acid protons, δ_{con} is zero and hence:

$$\delta_{dip}(obsd) = \delta_{obsd} - \delta_{dia} \quad (7)$$

The angles in the Euler rotation matrix, $\mathbf{R}(\alpha,\beta,\gamma)$, or both the rotation angles and magnetic anisotropies, are obtained through a three or five parameter least-square search for a minimum in the differences between an observed and calculated δ_{dip} for a set of n assigned resonances, as defined by the error function,[56] F/n:

$$\frac{1}{n}F(\alpha,\beta,\gamma\Delta\chi_{ax},\Delta\chi_{rh}) = \sum^{n}[\delta_{dip}(obsd) - \delta'_{dip}(calcd)\mathbf{R}(\alpha,\beta,\gamma)]^2 \quad (8)$$

where δ_{dip}(obsd) is provided by eq 7, and the calculated dipolar shift in the X-ray based pseudosymmetry coordinate system is obtained by eq 1. The search for a minimum in a three parameter fit to obtain only the Euler angles for selected input $\Delta\chi$ values was carried out over all space, with α from −180° to 180°, β from 0° to 90°, and γ from 0° to 180°, in 5° increments; near the minimum, the increment in angles was reduced to 1° for α and γ and 0.5° for β. Note that in this convention for the Euler angles only the magnitude, and not the sign[5], or β is relevant. For a five parameter search for the minimum F/n, the range in β was restricted to 0–20° within which F/n always exhibits a sharp minimum. The range of anisotropies included in the search are $\Delta\chi_{ax}$ from 1.02 to 1.32 × 10^{-33} m^3 and $\Delta\chi_{rh}$ from 0.20 to 0.70 × 10^{-33} m^3, each incremented by 0.01 × 10^{-33} m^3 near the minimum. The calculations were performed using the GLOBMIN program.[29]

The unit cell X-ray coordinates from the crystal structure of WT sperm whale MbCO are converted into the iron-centered pseudosymmetry coordinate system (x',y',z' in Figure 1) by the SMAX program. The position vectors for protons in metMbCN are readily available in the molecular coordinate system as provided by the X-ray structure of isostructural MbCO.[11] The program CALPS is used to obtain the calculated dipolar shift, δ_{dip}(calcd) (eq 2), with the pseudosymmetry coordinates (x',y',z') of the protons, the angle variable (α,β,γ), and the magnetic anisotropy ($\Delta\chi_{ax}$ and $\Delta\chi_{rh}$) as input. Simulation of the dipolar shifts due to the influence of systematic rotations of the magnetic axes of WT metMbCN were carried out using the CALPS program. The predicted shifts relative to DSS for various protons, are given by the following:

$$\delta_{pred} = \delta_{dia} + \delta_{dip}(calcd) \quad (9)$$

where δ_{dip}(calcd) is obtained via eq 2 using selected values for α, β, and γ. The computer programs SMAX, CALPS, and GLOBMIN, were written by S. D. Emerson for a Micro-VaxII station, as described in detail elsewhere.[29]

Results

Magnetic Susceptibility Tensor. A. Determination of Anisotropies. Previous 2D NMR studies of WT sperm whale metMbCN have afforded[14,15] the complete assignment of the heme and axial His F8 resonances, as well as the majority of the resonances that experience significant dipolar shifts (within 7.5 Å

(26) Dalvit, C.; Wright, P. E. *J. Mol. Biol.* **1987**, *194*, 313–327.
(27) Bundi, A.; Wüthrich, K. *Biopolymers* **1979**, *18*, 285–297.
(28) Cross, K. J.; Wright, P. E. *J. Magn. Reson.* **1985**, *64*, 220–231.
(29) Emerson, S. D. Ph.D. Thesis, University of California, Davis, 1989.

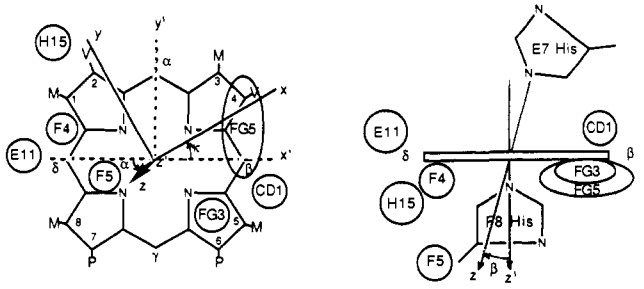

Figure 1. Schematic representation of the heme cavity: (A) face-on viewed from distal side, and (B), edge-on viewed from β-*meso*-H direction of sperm whale Mb based on the crystal structure of MbCO.[11] The general disposition of the proximal residues Leu F4, Ala F5, His F8, His FG3, Ile FG5, as well as the distal Phe CD1 and His E7, is given. Also provided are the numbering 1–8 of the pyrrole and α, β, γ, δ for the meso positions. The pseudosymmetry axes derived from the crystal structure are labeled x', y', z'. A general set of magnetic axes is described by the coordinate system x, y, z for which β describes the major magnetic or z-axis tilt from the heme normal, α (not related to α-meso position on heme) is the angle between the projection of the z-axis tilt on the heme plane and the x' axis (so that α is positive for counterclockwise rotation from the $-x'$ axis), the projection of the x' and y' (rhombic axes) on the heme plane is described by the angle $\kappa \sim \alpha + \gamma$. The major two coordinate systems are related by the standard Euler rotation $\mathbf{R}(\alpha,\beta,\gamma)$ where $[x,y,z] = [x',y',z']\mathbf{R}(\alpha,\beta,\gamma)$.

of the iron). Residues whose signals were found to be inappropriate because of demonstrated variable orientation and or mobility[14,15] were the side chains of Leu F4 and Val E11. The magnetic axes have been determined using 32 reliable dipolar shifts and theoretical anisotropies,[8] as reported in detail previously.[5] The assignment of five additional signals,[15] those from residues Ala E14 ($C_\alpha H$) and the side chain of Thr E10 ($C_\alpha H$, $C_\beta H$), Ala F5 ($C_\alpha H, C_\beta H_3$), now provide a total of 37 values of δ_{dip} for the search for $\mathbf{R}(\alpha,\beta,\gamma)$. The signals whose dipolar shifts were used are defined as data set A and are listed under A in Table I. Inclusion of the five new signals in a search for **R** (based on the calculated $\Delta\chi$ values) leaves the magnetic axes unchanged and marginally reduces the error function, F/n, from 0.25 to 0.22 (top of Table II). A five parameter search that includes simultaneous optimization for α, β, γ, $\Delta\chi_{ax}$, and $\Delta\chi_{rh}$ using the 37 input shifts (data set A) yields the anisotropies $\Delta\chi_{ax}(A) = 1.12 \times 10^{-33}$ m^{-3} and, $\Delta\chi_{rh}(A) = 0.376 \times 10^{-33}$ m^{-3}, with only minor changes in the rotation matrix (second entry in Table II). Hereafter we designate anisotropies determined experimentally from a five parameter search as $\chi_{ax}(J)$ and $\chi_{rh}(J)$, where J is one of the data sets A–F (Table I) used in the least-square search; the remaining $\Delta\chi(J)$ values angles, and F/n are listed in the lower portion of Table II.

B. Influence of Limited Data Sets. In setting the stage for determining the magnetic axes for point mutants, we first consider those detailed structural elements of the WT that could reasonably be retained in a mutant, so that their geometric factors in the metal-centered coordinate system can be transferred to a mutant. Second, we determine how well those restricted structural elements and their observed δ_{dip} can generate the magnetic axes and anisotropies for the WT metMbCN. A distal point mutation is likely to leave the globin (C_αHs) backbone essentially unperturbed. The proximal side chain orientations can be expected to be unaltered. While the distal side chain orientations are very likely perturbed, the highly conserved Phe CD1 appears to retain a largely unaltered disposition relative to the heme in a wide variety of ligation states of Mb that perturb the orientation of other distal residues.[11,12,30] Thus we construct a series of input data sets, B–E, that retain a variable degree of structure and number of input data points (n) for a least-square search: set B, proximal, Phe CD1, and E helix C_αHs (25); set C, proximal and Phe CD1 (22); set D, proximal only (19); set E, limited proximal (9), as well as a minimal set F which is restricted to five strongly relaxed, strongly

(30) Lionetti, C.; Guanziroli, M. G.; Frigerio, F.; Ascenzi, P.; Bolognesi, M. *J. Mol. Biol.* **1991**, *217*, 409–412.

Table II. Orientation of Magnetic Axes, Magnetic Anisotropies, and Error Functions for Least-Square Searchs for WT MetMbCN

input data sets		parameters[c]	magnetic axes orientation[d]			anisotropies[e]		error function[f]	
code[a]	n[b]		α	β	κ	$\Delta\chi_{ax}$	$\Delta\chi_{rh}$	F/n	F'/n
A	37	3	0	14.5	35	1.22[g]	0.476[g]	0.220	0.220
A	37	5	10	15.5	35	1.12[h]	0.376[h]	0.084	0.084
B	25	3	11	15.5	35	1.12[i]	0.376[i]	0.050	0.098
B′	20	3	11	15.5	33	1.12[i]	0.376[i]	0.051	0.095
C	22	3	10	15.5	35	1.12[i]	0.376[i]	0.066	0.099
C′	17	3	12	15.5	31	1.12[i]	0.376[i]	0.053	0.096
D	19	3	10	16.0	37	1.12[i]	0.376[i]	0.054	0.124
D′	14	3	9	16.0	39	1.12[i]	0.376[i]	0.055	0.134
E	9	3	10	16.0	36	1.12[i]	0.376[i]	0.057	0.122
F	5	3	7	15.5	35	1.12[i]	0.376[i]	0.067	0.106
B	25	5	11	15.5	35	1.12	0.396	0.048	0.100
C	22	5	14	16.0	35	1.07	0.396	0.054	0.097
D	19	5	10	15.5	35	1.09	0.396	0.052	0.12
D′	14	5	9	16.0	38	1.13	0.396	0.051	0.13
E	9	5	0	15.5	40	1.18	0.456	0.032	0.19
F	5	5	−5	15.0	40	1.22	0.476	0.017	0.24

[a] Set of observed δ_{dip} for the resonances as identified in Table I. [b] The number of observed δ_{dip} used in the search. [c] Number of parameters in least-square search: 3 (α, β, γ) or 5 (α, β, γ, $\Delta\chi_{ax}$, $\Delta\chi_{rh}$). [d] The angles in $\mathbf{R}(\alpha,\beta,\gamma)$, with $\kappa = \alpha + \gamma$. [e] $\times 10^{-33}$ m^{-3}. [f] F/n defined in eq 8 for the n input δ_{dip} used in the least-square search; F'/n is eq 8 but summed over the 37 available δ_{dip}. [g] Values computed from ligand field theory.[8] [h] The optimal anisotropies for the 37 input δ_{dip} data set A five parameter least-square search are referred to as $\Delta\chi_{ax}(A)$, $\Delta\chi_{rh}(A)$ in text. [i] Three parameter fits from restricted input NMR data sets are carried out using the $\Delta\chi_{ax}(A)$ and $\Delta\chi_{rh}(A)$ determined in the five parameter fit using all 37 experimental δ_{dip}.

shifted and well-resolved signals that are readily assigned without recourse to 2D methods. Several subsets (B′, C′, and D′) are also considered which omit five weakly shifted resonances that are not easily assigned in the present point mutants. The detailed composition of the various data sets A–F set out in Table I.

For each of the input data sets defined in Table I, a three parameter least-square search was made to obtain the $\mathbf{R}(\alpha,\beta,\gamma)$ that globally minimizes the error function F/n (eq 8), using $\Delta\chi_{ax}(A)$ and $\Delta\chi_{rh}(A)$ determined from the five parameter fit for the WT metMbCN using the complete 37 parameter input NMR data set, as well as $\Delta\chi$ values calculated by Horrocks and Greenberg[8] (not shown; see the supplementary material). Moreover, for each input data set, J = (A–F), a five parameter search was also executed in order to obtain $\mathbf{R}(\alpha,\beta,\gamma)$, $\Delta\chi_{ax}(J)$, and $\Delta\chi_{rh}(J)$ from each limited set. The resulting angles, α, β, the rhombic axes, $\kappa = \alpha + \gamma$ (Figure 1), the anisotropies, and the error functions, F/n, are listed in Table II. Two error function are given: F/n is the minimized value over the n input data used in the least-square search[5] and measures the quality of the fit based on the selected data. F'/n is the error function evaluated over all 37 available data points using the same magnetic axes and anisotropies that minimize F/n. Thus F'/n serves as a test for the relative quality of the orientation and anisotropies determined by limited input data sets.

The effect of using the calculated $\Delta\chi$ values versus $\Delta\chi_{ax}(A)$ and $\Delta\chi_{rh}(A)$ with the various data sets in Table I leads to only minor differences in orientation (range in $\beta < 1°$, $\alpha \sim 10°$, $\kappa = \alpha + \gamma < 5°$) but always to a much larger error function (i.e., poorer fit) using the calculated $\Delta\chi$ values (shown only for set A in Table II; see the supplementary material for additional data). Moreover, all trends for $\mathbf{R}(\alpha,\beta,\gamma)$ with variable input data sets were the same using either calculated $\Delta\chi$ values or our presently determined values. Hence we do not further consider analyses based on the calculated $\Delta\chi$ values. Using the $\Delta\chi(A)$ values from the 37 input data point five parameter search, a comparison of the $\mathbf{R}(\alpha,\beta,\gamma)$ determined in a three parameter search using the various restricted data sets reveals that the determined orientation is largely independent of which input data is used (Table II). The ranges in α, β, and κ are 5°, 0.5°, and 8°, respectively. There is clearly a remarkable consistency considering that the number

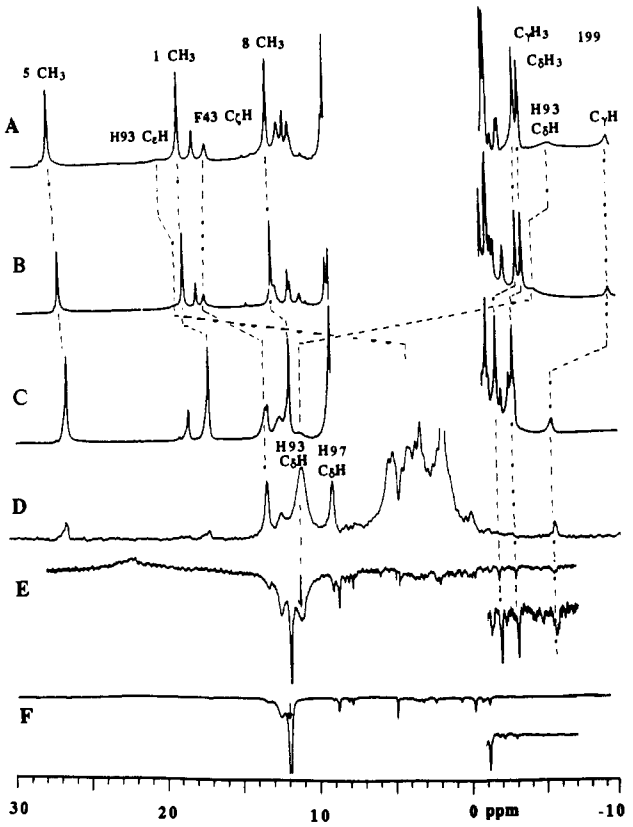

Figure 2. 500-MHz ^{1}H NMR spectra of metMbCN complexes in ^2H_2O, pH 8.6, at 25 °C for the following: (A) Arg CD3 → Gly mutant, (B) wild type, (C) His E7 → Gly mutant. Some of the previously reported assignments for WT metMbCN are given, and the correlation with the two mutants established in this work are given by dashed lines. (D) The trace for the E7 Gly mutant collected under rapidly pulsing conditions (20 s^{-1}) that emphasizes rapidly relaxing signals. (E) Saturation of broad His F8(93) ring proton signal; note NOEs to Ile FG5(99) $C_\gamma H3$, $C_\delta H3$, and $C_\gamma H$, as expected for the F8(93) $C_\delta H$ in the crystal structure. (F) Saturation of 8-CH_3 peak shows that Ile FG5(99) NOEs in trace E are not from off-resonance saturation.

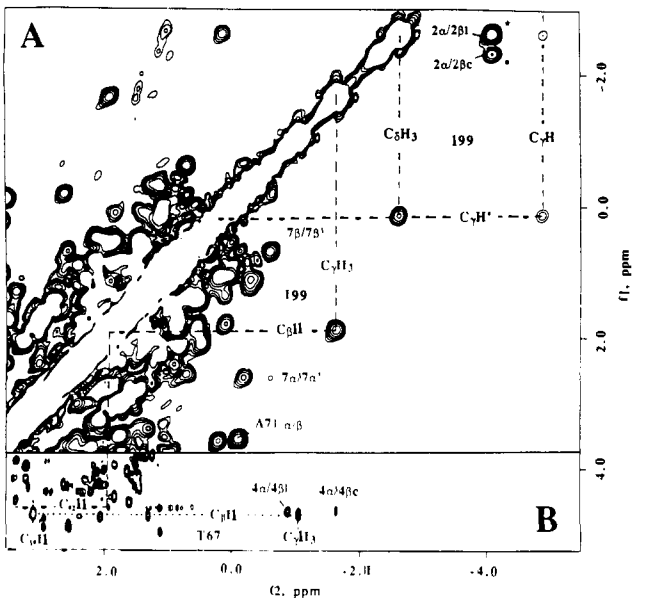

Figure 3. Upfield portions of the magnitude COSY map of E7 Gly metMbCN in ^2H_2O, pH 8.6, at 40 °C. (A) Cross peaks from Ile FG5-(99) (dashed lines), Ala E14(71), and heme 7-propionate and 2-vinyl groups are shown. The low-field 2-vinyl H_α peak is folded in from 18 ppm; the cross peaks are labeled by asterisks. In order to enhance the weak cross between broad resonances, the map was processed by zero phase-shifted sinebell-squared window function over 256 t_1 and t_2 points. (B) Cross peaks from Thr E10(67) (dotted lines) and the heme 4-vinyl group. This portion of the map was processed by apodizing over 1024 t_2 and 418 t_1 points to maximize resolution. The heme peaks are listed by the standard numbering in Figure 1B. The amino acid peaks are designated by the standard letter code and the description of side chain protons.

of input shifts varies from 37 to only 5! Moreover, the orientation is essentially unaffected whether the experimental δ_{dia} from WT MbCO or the calculated δ_{dia} (eq 6) were used, although the former yielded a slightly lower error function. When the least-square search is extended to all five parameters to additionally obtain anisotropies, the range of orientations is not extended significantly. It can therefore be expected that the various limited input data sets for residues unperturbed by distal mutation, in particular data sets D, D′, E in Table I, should allow the accurate determination of the magnetic axes for point mutants.

Assignment of Point Mutant NMR Spectra. The resolved portions of the 500-MHz ^{1}H trace of the CD3 Gly, WT, and E7 Gly forms of metMbCN in ^2H_2O are illustrated in parts A, B, and C respectively of Figure 2; several assignments for WT metMbCN[14,15] are given. The shifts for the prominent three low-field heme methyl signals appear largely unchanged among the three proteins. Comparison of the spectra reveals only very slight differences between the spectra of the WT and CD3 Gly mutant metMbCN complexes (although a general pattern is that strongly hyperfine shifted non-heme signals are very slightly further from the diamagnetic envelope in the mutant than in the WT). For the E7 Gly metMbCN mutant, there is a general and substantial decrease in the hyperfine shifts of all non-heme resonances. The ^{1}H trace for this protein collected under rapid pulsing conditions that emphasize broad, rapidly relaxing signals is shown figure 2D; only one of the two broad His F8 ring protons is resolved with significantly perturbed shift as compared to either of these two peaks in WT.[14] We pursue below the detailed assignment needed for the magnetic axes determination for the perturbed E7 Gly met MbCN spectrum. While similarly definitive experiments were carried out on the CD3 Gly metMbCN mutant, the assignments could have been made completely by comparison to the WT spectrum since the shift changes are small. 2D NMR data relevant to CD3 Gly metMbCN assignments are provided in the supplementary material.

A. Heme Protons. The COSY map of E7 Gly metMbCN reveals the characteristic cross peak patterns for two vinyl[31] (Figure 3A,B) and two propionate groups (Figures 3A, and 4A). The resolved heme 1-CH_3 peak is assigned on the basis of a NOESY cross peak to both a vinyl (2-vinyl) (Figure 5) and 8-CH_3 (not shown). This assigns also the 4-vinyl and the adjacent 3-CH_3 (Figures 3B, 6A). The remaining low-field methyl must be the 5-CH_3 whose NOEs reveal the 6-propionate resonances (Figure 5). An upfield four-spin system (Figure 3A) with NOESY cross peaks to 8-CH_3 (Figure 5) identifies the 7-propionate group. The four *meso*-H are readily identified by the simultaneous NOESY cross peak to the pair of adjacent pyrrole substituents (Figures 5 and 6) and their characteristic strong low-field bias with increasing temperatures[14] (not shown). The observed heme shifts reveal a very similar hyperfine shift pattern that is dominated by the larger contact shifts.[2,5] Moreover, the largely unaltered heme methyl shift pattern, which is determined by the rhombic orbital ground state,[2,9] supports in-plane rhombic axes that are not significantly changed from that of the WT. The heme chemical shifts for the two mutants, as well as WT metMbCN, are provided in the supplementary material. The chemical shifts for assigned amino acid signals for the two mutants are listed in Table III along with those for WT metMbCN; T_1 values for resolved resonances of E7 Gly metMbCN are also included.

B. Proximal Residues. The upfield COSY map exhibits cross peaks from resolved CH_2–CH_3 and CH–CH_3 fragments (Figure 3A) which the NOESY map (Figure 6) reveals to be in close dipolar contact and which must originate from Ile FG5(99). The

(31) The 2-vinyl H_α peak at 18.3 ppm is folded in to −4 ppm to improve the digitization; the two folded in cross peaks to 2-$H_{\beta c}$, 2-$H_{\beta 1}$ are marked by asterisks.

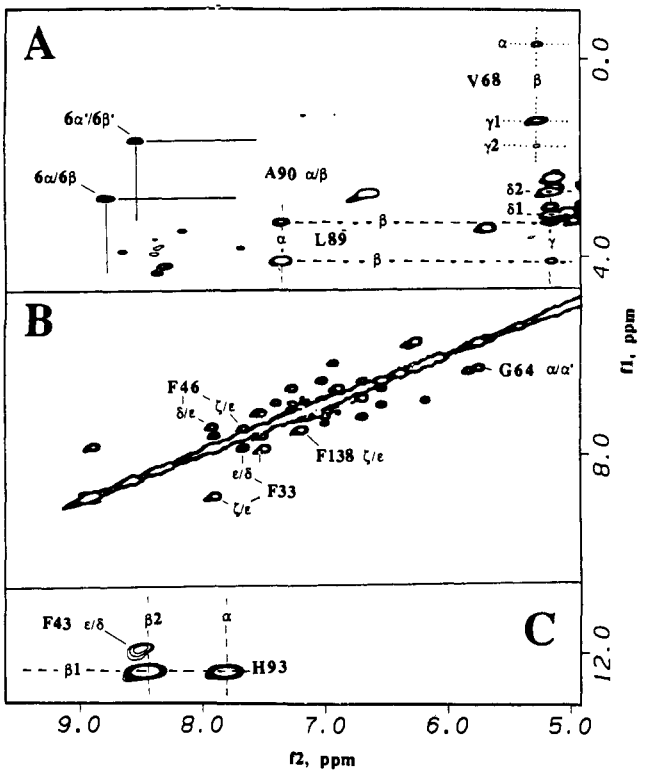

Figure 4. The low-field portions of the magnitude COSY map of E7 Gly metMbCN in ^2H_2O, pH 8.6, at 30 °C (A and B) and at 40 °C (C). (A) The cross peaks for the spin systems Leu F4(89) (dashed lines), Ala F5(90) and Val E11(68) (dotted lines), and the heme 6-propionate group (solid lines) are labeled. This portion of the map was apodized over 512 $t_1 \times 512$ t_2 points to enhance weak cross peaks between the broad resonances. (B) Cross peaks from Gly E7(64), 6-propionate, Phe B14(33), Phe CD4(46), and Phe H15(138). This portion of the map was apodized over 1024 t_2 and 512 t_1 points to enhance resolution near the diagonal. (C) Cross peaks for His F8(93) (dotted lines) and the one detected cross peak for Phe CD1(43). This portion was processed by applying a sine-bell-squared window function over 256 points in both t_1 and t_2 dimensions. All cross peaks were observed over ranges of temperature to confirm the unique connectivities.

C_β–$C_\gamma H$ cross peaks are not detected because of the small coupling constants and resulting weak cross peaks, as found in WT.[15] The additional $C_\beta H$ COSY cross peak locates the remaining $C_\alpha H$. The conserved orientation of the Ile FG5(99) side chain is confirmed by observing a pattern of intra-residue NOESY cross peaks that is essentially identical to that of WT metMbCN[14] (Figures 5 and 6). The unchanged disposition of Ile FG5(99) relative to the heme periphery and iron center is confirmed by the identical pattern of inter-residue NOESY cross peaks (i.e., $C_\delta H_3$:5-CH_3, $C_\delta H_3$:β-*meso*-H, $C_\gamma H_3$:3-CH_3, $C_\gamma H_3$:4H_α) and unaltered paramagnetic relaxivities[14,32] ($C_\gamma H$, $T_1 \sim 72$ ms).

A characteristic three-spin COSY and NOESY pattern in the low-field region locates the His F8(93) $C_\beta H_2$–$C_\alpha H$ fragment (Figure 4C), as confirmed by a NOESY cross peak from $C_\alpha H$ to Ile FG5(99) $C_\delta H_3$ (Figure 5), as expected and observed[14,15] in WT metMbCN. The sole resolved broad F8 ring proton fails to yield NOESY cross peaks. However, saturating this resonance under rapid pulsing conditions (Figure 2E) yields NOEs to Ile FG5 $C_\delta H_3$, $C_\gamma H_3$, and $C_\gamma H$, as expected and observed in WT metMbCN[14] for the F8 $C_\delta H$. Saturation of the 8-CH_3 (Figure 2F) serves as a control to show that the NOEs to Ile FG5 arise from the broad resonance. The intensity distribution in the reference spectrum collected under rapidly pulsing conditions (Figure 2D) dictates that the F8 $C_\epsilon H$ must resonate in the 2–7 ppm region; i.e., 4.5 ± 2.5 ppm. The spectrum in Figure 2D also reveals another rapidly relaxing proton at ~9 ppm with a $T_1 \sim 20$ ms; the NOESY peak to His F8 $C_\alpha H$ (Figure 5) and characteristic T_1 identify it as His FG3(97) $C_\delta H$ with the same disposition[14] as in the WT metMbCN. The His FG3 $C_\epsilon H$ is readily identified by its characteristic[14] NOE to 6-H_α. The β-methylene protons for this residue appear in too crowded a region to make definitive assignment possible. A NOESY cross peak from His F8 $C_\beta H$ to a proton (Figure 5), together with a single COSY cross peak (Figure 4), locates the $C_\alpha H$ and $C_\beta H_3$ of Ala F5(90). A complete Leu spin system is located in the COSY map (Figure 4), and NOEs from this spin system to the heme 1-CH_3 (Figure 5A) identify[15] it as Leu F4(89). NOESY cross peaks from 1-CH_3 and 2-H_α to the aromatic region (Figure 5A), together with a COSY cross peak among these resonances (Figure 4B), identify[14,15] Phe H15(138). All of the above resonances exhibit the identical NOESY and COSY connectivity patterns described for WT metMbCN,[14,15] except that the shifts for many of the resonances are altered.

(32) The parametic relaxivity, $T_{1i}^{-1} \propto R_i^{-6}$; where R_i is the distance to the iron. the presently observed T_1 value is within experimental uncertainty of that (65 ± 7 m) reported from WT metMbCN.

Table III. ^1H NMR Spectral Parameters for WT and Arg CD3 → Gly and His E7 → Gly mutant metMbCN[a]

residue	peak	WT shift[b]	Arg CD3 → Gly shift	His E7 → Gly shift	His E7 → Gly T_1[c]
Leu F4(89)	$C_\alpha H$	8.53	8.50	7.36	
	$C_\beta H$	3.82	3.75	3.33	
	$C_\beta H'$	4.44	4.36	4.10	
	$C_\gamma H$	5.87	5.99	5.16	
	$C_{\delta 1}H_3$	3.93	3.91	3.15	
	$C_{\delta 2}H_3$	3.25	3.13	2.69	
Ala F5(90)	$C_\alpha H$	6.40	6.32	6.64	
	$C_\beta H_3$	2.63	2.59	2.73	
His FG3(97)	$C_\delta H$	10.79	10.94	8.82	20
	$C_\epsilon H$	6.84	7.01	6.17	
Ile FG5(99)	$C_\alpha H$	2.38	2.29	3.14	
	$C_\beta H$	−0.09	−0.19	1.91	
	$C_\gamma H$	−9.23	−9.37	−5.36	72
	$C_\gamma H'$	−1.78	−1.86	0.06	
	$C_\gamma H_3$	−3.34	−3.45	−1.83	179
	$C_\delta H_3$	−3.70	−3.75	−2.90	173
Phe H15(138)	$C_\delta Hs$	7.02	7.08	7.10	
	$C_\epsilon Hs$	6.94	6.90	7.22	
	$C_\zeta H$	7.05	7.08	7.55	
His F8(93)	$C_\alpha H$	7.43	7.36	8.09	
	$C_\beta H$	11.40	11.23	12.88	
	$C_\beta H'$	6.34	6.05	8.80	
	$C_\delta H$	−4.3	−5.6	10.9	~4
	$C_\epsilon H$	18.8	19.7	4.5±2.5	
Phe CD1(43)	$C_\delta Hs$	8.65	8.49	8.57	
	$C_\epsilon Hs$	12.39	12.03	12.26	
	$C_\zeta H$	16.93	16.67	13.12	22
Thr E10(67)	$C_\alpha H$	2.50	2.58	3.05	
	$C_\beta H$	2.68	2.67	4.71	
	$C_\gamma H_3$	−1.49	−1.60	−1.23	186
Val E11(68)	$C_\alpha H$	−2.36	−2.30	−0.26	
	$C_\beta H$	1.44	1.52	5.28	
	$C_{\gamma 1}H_3$	−0.97	−0.76	1.27	
	$C_{\gamma 2}H_3$	−0.81	−0.17	1.79	
Ala E14(71)	$C_\alpha H$	3.48	3.53	3.49	
	$C_\beta H_3$	−0.09	−0.11	−0.28	
His E7(64)	$C_\delta H$	11.57	11.69		
Gly E7(64)	$C_\alpha H$			5.83	
	$C_\alpha H'$			6.33	
Phe B14(33)	$C_\delta Hs$	7.96	7.94	7.68	
	$C_\epsilon Hs$	8.31	8.30	7.91	
	$C_\alpha H$	8.31	8.30	8.89	
Phe CD4(46)	$C_\delta Hs$	7.64	7.85	7.92	
	$C_\epsilon Hs$	7.98	8.05	7.50	
	$C_\zeta H$	7.64	7.85	7.66	

[a] Chemical shifts in ppm from DSS, at 30 °C, pH 8.6. [b] Data taken from ref 14. [c] For resolved resonances, in ms; uncertainty ±10%.

C. Conserved Distal Residues. The most prominent distal residue is Phe CD1(43) whose aromatic ring gives rise to a strongly

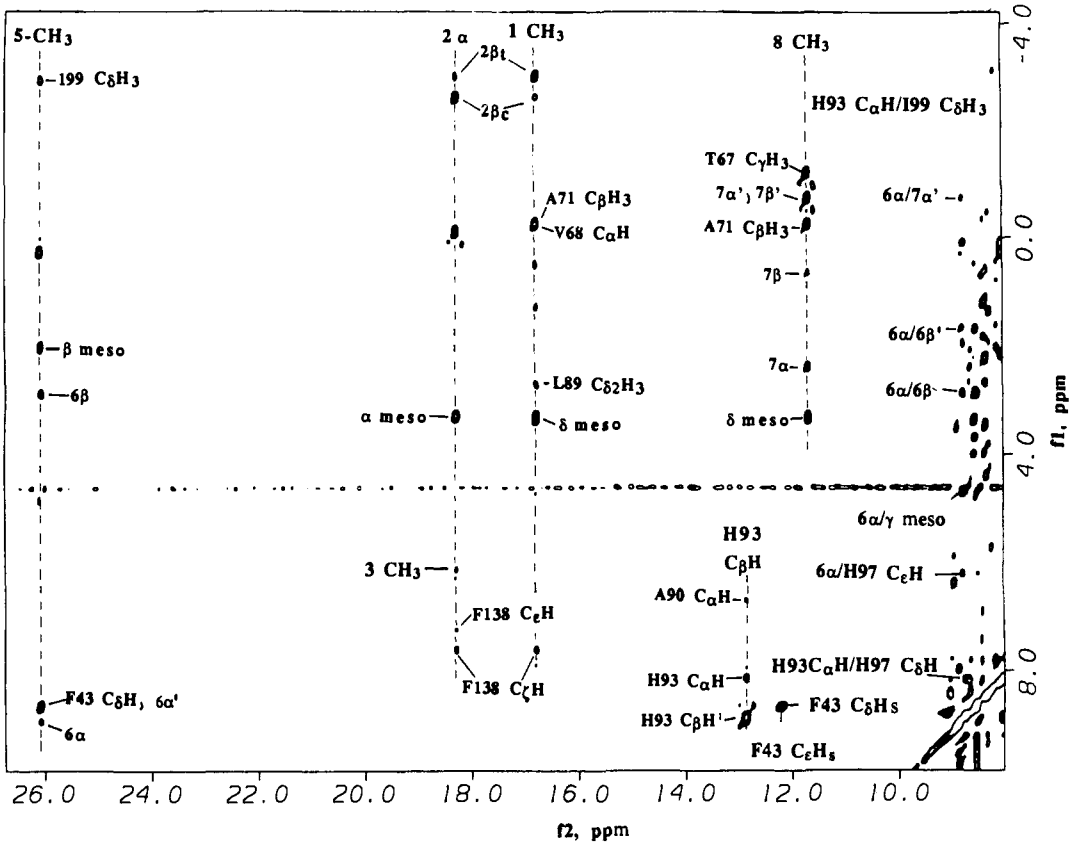

Figure 5. Low-field portion of the NOESY map collected with a 50-ms mixing time for E7 Gly metMbCN in ^2H_2O, pH 8.6, at 30 °C. For the resolved 5-CH_3, 1-CH_3, 2-H_α, His F8 $C_\beta H$, and 8-CH_3 resonances (shown by vertical dashed lines) cross peaks are labeled only in the $f1$ dimension, with the common $f2$ label given above or below the dashed line. Other cross peaks are labeled by the appropriate resonances in the $f2/f1$ dimensions. The standard one-letter amino acid codes and side chain descriptions are used.

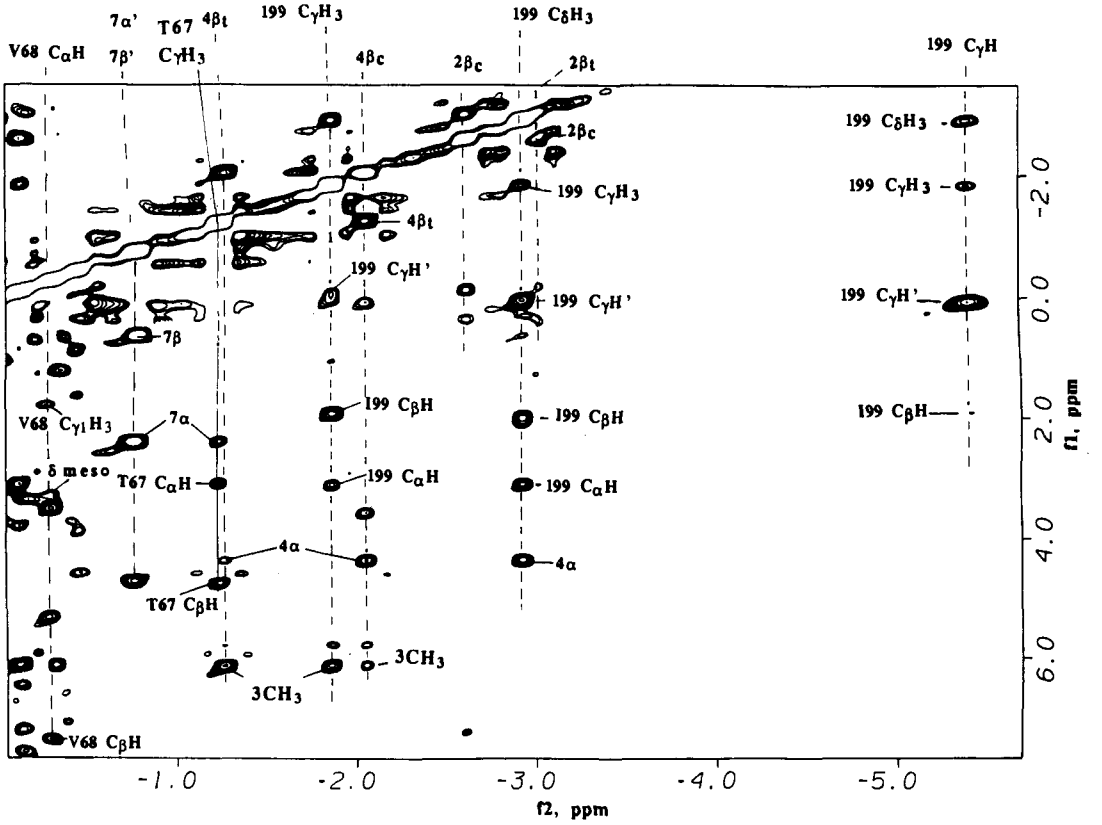

Figure 6. Upfield portion of the NOESY map, collected with 50-ms mixing time, for E7 Gly metMbCN in ^2H_2O, pH 8.6, at 30 °C. The Ile FG5(99) resonance, Thr E10(67), Val E11(68), and heme vinyl are identified by vertical lines along the $f1$ dimension, with the peak labeled above or below the line. The cross peaks are therefore labeled only by the appropriate $f1$ dimension.

low-field shifted single proton peak,[14,33] C_fH, with characteristic T_1 ~20 ms. This peak exhibits a 1D NOE to an averaged two-proton signal, $C_\epsilon Hs$ (not shown), which itself exhibits a COSY peak to the $C_\delta Hs$ (Figure 4C). The NOESY peak between $C_\delta Hs$ and 5-CH_3 (Figure 5) and 1D NOE to $4H_\alpha$ (not shown), together with unchanged relaxivity[32] compared to WT metMbCN (C_fH T_1 ~20 ms), confirm the Phe CD1 assignment[33] and establish the same orientation as that in WT metMbCN.[14] A strong NOESY peak from 1-CH_3 and 8-CH_3 to a peak at −0.28 ppm locates the Ala E14(70) $C_\beta H_3$ (Figure 5); a single COSY cross peak to 3.49 ppm locates the $C_\alpha H$ (Figure 3). An additional NOESY cross peak from 8-CH_3 to a resolved upfield methyl (Figure 5), which is part of a three-spin system (Figure 3A) with the $C_\alpha H$ at 3.05 ppm, identifies Thr E10(67); NOEs to the 7-propionate are observed from $C_\gamma H_3$, as expected from the WT crystal coordinates[11] (Figure 6). An NOE to an upfield-shifted one proton signal from the 1-CH_3 (Figure 5) shows it to be $C_\alpha H$ of a member of a spin system diagnostic of a Val (Figure 6) which must be Val E11(68).[14,15] 1D NOEs from Phe CD1 $C_\epsilon Hs$ to the aromatic region reveal four largely temperature insensitive signals (not shown); the complete spin systems are defined in the COSY map and identify two Phe that must be from B14(33)/CD4(46) (Figure 4B), the only other nonassigned aromatic side chains near the heme pocket. The B14 and CD4 spin systems are differentiated[14] on the basis that the more intense 1D NOEs from Phe CD1 $C_\epsilon H$ occur for Phe B14.

D. The Substituted Distal Residue. The 1D saturation of the assigned Thr E10(67) $C_\gamma H_3$ signal over a range of temperatures reveals very weak NOEs (not shown) to two protons with temperature-sensitive shifts which themselves exhibit a strong COSY and NOESY peak at each of the temperatures (Figure 4B). The only methylene group in the proximity of the Thr E10(67) $C_\gamma H_3$ is the E7 Gly(64) $C_\alpha H_2$. The E10 $C_\gamma H_3$ to E7 $C_\alpha H$ distance in WT Mb[11] is ~5 Å, consistent with the observed NOE.[34]

The temperature dependence of all noncoordinated amino acid signals yielded a slope in the Curie plot (shift versus reciprocal temperature) which is proportional to the observed dipolar shift (not shown; see the supplementary material). This correlation can be taken as evidence for a unique orientation for each residue, as discussed previously for WT metMbCN.[5]

Magnetic Axes Determination in Point Mutants. The determination of the magnetic axes for the distal point mutants makes the assumption that both the crystal coordinates and δ_{dia} for solely proximal side residues are inconsequentially changed from those of the WT protein: the distal side coordinates and δ_{dia} need not, and are not expected to, be conserved. The assumption of a conserved proximal side of the heme in spite of a distal point mutation is based on the observation in WT Mbs that strong distal perturbations leave the proximal pocket unaltered. Thus in sperm whale Mb, the proximal coordinates are essentially the same whether the small CO ligand is bound to the reduced form[11] or a bulky phenyl group that keeps the distal pocket pocket open is coordinated to the iron in the oxidized protein.[22] For the related *Aplysia* Mb, three crystal studies reveal highly differential penetration of the distal pocket by an unconventional residue to hydrogen bond to the distal ligand[35] but leave the proximal side unaltered. Preliminary crystal coordinates for the E7 Gly Mb mutant[36] support the premise that significant structural perturbations are restricted to the distal side.

The assignment of the mutant metMbCN spectra failed to provide unambiguous assignments for the His FG3(97) $C_\beta Hs$, the Leu G5(108) $C_\gamma H$ and $C_{\delta 2}H_3$, and Tyr H23(146) $C_\epsilon Hs$, providing five less proximal shifts than for the WT protein,[5,14,15] i.e., data sets B′, C′, and D′, as well as the sets E and F which are identical to those used for WT. However, a comparison of the **R** and F/n for any pair of data sets differing in these five signals for WT leads to insignificant differences in **R** (0° in β, 2° in α, and 4° in κ) and F/n (Table II). The three parameter least-square searches for the magnetic axes for both mutants based on the input of dipolar shift data sets B′, C′, D′, E, and F of Table I, using the $\Delta\chi_{ax}(A)$ and $\Delta\chi_{rh}(A)$ from the five parameters fit for the WT using 37 data points, lead to well-defined minima in F/n and low values of the error function. When the least-square search is extended to five parameters for the E7 Gly mutant to obtain $\Delta\chi$ values using the largest proximal data set D′, the resulting $\Delta\chi_{ax}$ is unchanged from $\Delta\chi_{ax}(A)$ and $\Delta\chi_{rh}$ minimally changed from $\Delta\chi_{rh}(A)$. The resulting Euler angles and F/n are listed in Table IV. For both mutants, the searches using different input data sets yield remarkably consistent magnetic axes (ranges in β of 1°, α of 5°, and κ of 6°). For the CD3 Gly mutant, the axes appear unchanged from those of the WT. The E7 Gly mutant, however, reveals a strongly perturbed orientation with a minimal change in the degree of tilt (β), but a significant (~45°) rotation of the direction of the tilt (α). What is remarkable is that, like in the WT, the magnetic axes in the mutants are as well determined with minimal input data set F as with the most extensive data set D′.

Table IV. Orientation of Magnetic Axes, Magnetic Anisotropies, and Error Functions, for Least-Square Searches for metNbCN Point Mutants

input data sets		para-	magnetic axes orientation[d]			anisotropies[e]		error function[f]
code[a]	n[b]	meters[c]	α	β	κ	$\Delta\chi_{ax}$	$\Delta\chi_{rh}$	F/n
			His E7 → Gly Mutant					
B′	20	3	−30	13.0	48	1.12	0.376	0.072
C′	17	3	−31	13.5	46	1.12	0.376	0.067
D′	14	3	−34	13.5	43	1.12	0.376	0.031
D′	14	5	−34	13.5	42	1.12	0.340	0.023
E	9	3	−35	13.5	42	1.12	0.376	0.031
F	5	3	−31	14.0	46	1.12	0.376	0.051
			Arg CD3 → Gly Mutant					
B′	20	3	12	15.0	20	1.12	0.376	0.094
C′	17	3	13	15.0	26	1.12	0.376	0.071
D′	14	3	11	16.0	36	1.12	0.376	0.043
E	9	3	11	16.0	36	1.12	0.376	0.060
F	5	3	9	15.0	30	1.12	0.376	0.063

[a] Set of observed δ_{dip} for resonances as defined in Table I. [b] Number of observed δ_{dip} used in the search. [c] Number of parameters in least-square search: 3 (α,β,γ) or 5 ($\alpha,\beta,\gamma,\Delta\chi_{ax},\Delta\chi_{rh}$). [d] Angles in $\mathbf{R}(\alpha,\beta,\gamma)$ with $\kappa = \alpha + \gamma$. [e] The $\Delta\chi_{ax}(A)$ and $\Delta\chi_{rh}(A)$ values obtained from the five parameter least-square search using 37 δ_{dip} (data set A) for WT metMbCN (second entry in Table II) are used in all cases except for data set D′ in the five parameter search for E7 Gly metMbCN. [f] F/n defined in eq 8 for the n input $\delta_d 3i_p$ used in the least-square search.

Simulation of NMR Spectra as a Function of $\mathbf{R}(\alpha,\beta,\gamma)$. Equation 2 together with the least-square determined magnetic axes and anisotropies of WT metMbCN, allows the prediction (via eq 8) of all changes in the NMR spectrum of WT metMbCN based on systematic controlled changes in orientation of the magnetic axes. Such simulations identify which resonances can differentiate between changes in α and β in the rotation matrix and serve as a basis for quantitative analysis of very small changes in orientation of the magnetic axes (see below). Thus the δ_{dip} are calculated as a function of α (β constant) or β (α constant) while keeping the rhombic axes ($\kappa \sim \alpha + \gamma$) invariant. For the His F8(93) residue, the shift changes are calculated only for the dipolar part, and it is assumed that the contact shifts, δ_{con}, are unchanged from those in the WT,[37] as reported previously.[5] This assumption is reasonable since the predicted shift for the F8 ring for zero tilt

(33) Emerson, S. D.; Lecomte, J. T. J.; La Mar, G. N. *J. Am. Chem. Soc.* **1988**, *110*, 4176–4182.

(34) While a somewhat shorter T_1 for the Thr E10 $C_\gamma H_3$ (~180 ms) than in WT metMbCN (280 ms) reflects some minor reorientation, even ±60° rotation about C_α–C_β bond does not significantly increase the $C_\gamma H_3$ distance to the E7 $C_\alpha Hs$.

(35) Bolognesi, M.; Onesti, S.; Gatti, G.; Coda, A.; Ascenzi, P.; Giacometti, A.; Brunori, M. *J. Mol. Biol.* **1989**, *205*, 529–544. Bolognesi, M.; Coda, A.; Frigerio, F.; Gatti, G.; Ascenzi, P.; Brunori, M. *J. Mol. Biol.* **1990**, *225*, 621–625. Mattevi, A.; Gatti, G.; Coda, A.; Rizzi, M.; Ascenzi, P.; Brunori, M.; Bolognesi, M. *J. Mol. Recognit.* **1991**, *4*, 1–6.

(36) Phillips, G. N. Personal communication.

(37) The δ_{con} for $C_\epsilon H$, $C_\delta H$, $C_\beta H$, and $C_\beta H'$ for WT metMbCN are −17.8, −2.5, 5.6, and −2.2 ppm, respectively.

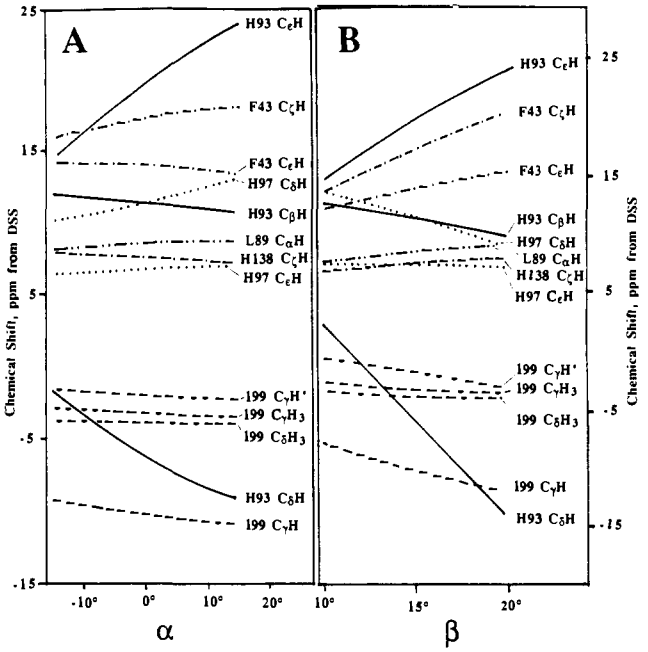

Figure 7. Simulation of the perturbations of the ^{1}H NMR shifts of WT metMbCN based solely on changes in the dipolar shift predicted by (A) change in β for fixed $\alpha = 10°$ and fixed $\kappa \sim \alpha + \gamma = 40°$ and (B) change in α for β fixed at 14.5° with $\kappa \sim \alpha + \gamma$ held constant at 40°. The resonances are indicated by solid lines for His F8(93) (—), dashed lines for Ile FG5(99) (----), dotted lines for His FG3(97) (····), dash–dash–dot (- - -) for Phe H15(138), and dash–dot (-·-·-) for Phe CD1(43). The particular proton of each residue is identified on the appropriate drawn lines. The trend in predicted shifts for increase in α or β is the same for His F8(93) C_ζH and C_ϵH and all four Ile FG5(99) signals, but it differs from the His F8(93) C_βH, His FG3(97) C_δH and C_ϵH, and Phe H15-(138) C_ζH.

($\beta = 0$) in metMbCN have been shown[5] to be essentially the same as in a model compound.[38] Direct calculations of δ_{con} for the two mutants confirm this quantitatively (see the supplementary material). The predicted changes in shifts for relevant resonances in the metMbCN spectrum as a function of α and β are illustrated in Figure 7A and 7B, respectively. Inspection of Figure 7 reveals that the dipolar shift increases monotonically with more positive α or β for the resonances of His F8(93) ring CHs, Phe CD1(43) C_ζH, the four Ile FG5(99) resonances, and F4(89) C_αH. Hence change in shifts for these signals will not differentiate between changes in α versus β. The resonances for His FG3(97) C_δH, Phe H15(138) C_ζH, and His F8(93) C_βH, on the other hand, predict shifts in opposite direction for increasingly positive α or β and hence serve as key probes to differentiate between changes in α or β.

Another conclusion that can be drawn from Figure 7 is that, either an increase in β or a more positive α leads to a strong upfield bias for the His F8 C_δH and a strong lowfield bias for the C_ϵH. Therefore the pattern of His F8 ring hyperfine shifts does not serve as a unique probe for z-axis tilt as originally proposed.[5] However, since the F8 ring protons are most sensitive to change in either α or β because of their proximity to the iron, change in the shifts of these signals in a mutant is a clear indication that the magnetic axes have been altered. Moreover, we show later that the nature of the His F8 shift changes serves as an important confirmation for the magnetic axes obtained from the least-square search.

Discussion

Determination of Magnetic Anisotropy. The inclusion of the two anisotropies in the 37 data set input least-squares search for WT metMbCN leads to a significant decrease in the error function (from 0.22 to 0.084). The excellent correlation between the observed and predicted δ_{dip} (based on the proximal data set D in Table I) is clearly seen in the plot in Figure 8A. We conclude therefore that the $\Delta\chi_{ax}$ and $\Delta\chi_{rh}$ determined for WT metMbCN from a complete set of NMR data are more reliable than those based on ligand field calculations[8] using the lowest Kramers doublet g values.[13] The error function, however, is more sensitive to variation in $\Delta\chi_{ax}$ than variation in $\Delta\chi_{rh}$, with a change in axial anisotropy producing a 4-fold larger increase in F/n than a similar fractional change in rhombic anisotropy. Hence, the axial anisotropy is always more accurately determined by the NMR data than is the rhombic anisotropy. A rationalization for this observation is readily apparent. The rhombic (second) term in eq (1) makes a significant contribution to δ_{dip} only for protons near the heme plane because of the $\sin^2\theta$ term. However, since δ_{dip} used in the fit must be from a noncoordinating residue, the large heme moiety places the closest residues near the heme plane >7 Å from the iron due to van der Waals contact with the heme periphery. The axial term maximizes near the heme normal due to its $\cos^2\theta$ dependence, and noncoordinated residues approach the iron to 4.5 Å. Hence both the r^{-3} and angular dependence keep the rhombic contribution to δ_{dip} small relative to the axial term and leads to the much weaker sensitivity of the fit to $\Delta\chi_{rh}$.

The determination of $\Delta\chi$ values based on more restricted NMR data sets (B–F in Table II) for WT metMbCN leads to $\Delta\chi_{ax}$ and $\Delta\chi_{rh}$ intermediate between the theoretical values and the $\Delta\chi$(A) values determined from data set A. However, since the error function, F'/n (over all 37 available δ_{dip}), using the $\Delta\chi$ values for any of the restricted data set five parameter fits is smaller than that for the three parameter least-square search with 37 δ_{dip} and

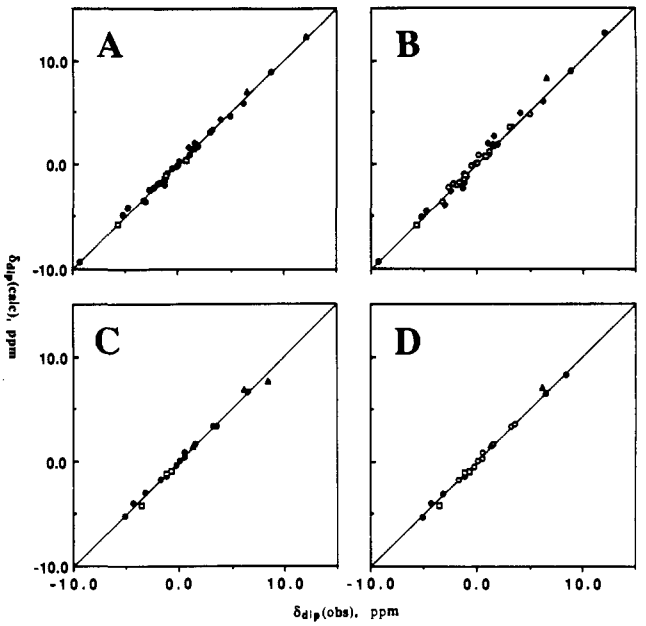

Figure 8. Plots of the predicted versus observed dipolar shifts; solid lines with unit slope represent a perfect fit. (A) WT metMbCN for the magnetic axes obtained from the 19 proximal residue signals (data set D in Table I). The input shifts are marked by a closed circle (●); distal C_αH, Phe CD1, and the remaining distal protons not used in the magnetic axes determination are marked by open square (□), closed triangle (▲), and open diamond (◇), respectively. (B) WT metMbCN for the magnetic axes obtained from the 5 input minimal data set (set F in Table I). The input data are given by a closed circle (●). Other proximal, distal C_αH, Phe CD1, and other distal protons not included in the least-square search are given by open circle (○), open square (□), closed triangle (▲), and open diamond (◇), respectively. (C) E7 Gly metMbCN for the magnetic axes obtained from the 14 point proximal residue data set (set D′ in Table I). The input shifts are shown in closed circles (●); distal C_αHs and the Phe CD1(43) proton signals are shown in open squares (□) and open triangels (△), respectively. (D) E7 Gly metMbCN for the magnetic axes determined from the 5 point minimal input data set (F in Table I). The input data are shown in closed circles (●). The remaining proximal residue (○), distal C_αHs (□), and Phe CD1(43) (△) residue signals are designated by open circles, open squares, and open triangles, respectively.

(38) Chacko, V. P.; La Mar, G. N. *J. Am. Chem. Soc.* **1982**, *104*, 7002–7007.

the fixed theoretical value of $\Delta\chi$, it appears that any of the more limited data sets yields a $\Delta\chi_{ax}$ more reliable than the theoretical value. We conclude, therefore, that the quantitative analysis of NMR dipolar shifts can provide a more accurate estimate of the paramagnetic anisotropies than provided by ligand field calculations[8] based on the lowest Kramers doublet g values.[13] Upon extending the determination of the magnetic axes to a distal mutant, the one case where a five parameter search was executed, (data set D' for E7 Gly metMbCN), $\Delta\chi$ values obtained are essentially identical to $\Delta\chi$(A) values (Table III). From this we conclude that the magnetic susceptibility tensor components of the two mutants are essentially unchanged from that of WT metMbCN. This conclusion that the anisotropies are unaltered is supported by the observation that the two high-field g values for E7 Gly metMbCN (3.44 and 2.06)[39] are essentially the same as those of WT metMbCN (3.45 and 1.99).[13]

Determination of the Magnetic Axes. The quality of any fit for WT metMbCN, as measured by either F/n or F'/n, is most sensitive to changes in β, the z-axis tilt and much less sensitive to α or γ. Using the data set A input parameters and the $\Delta\chi$(A) values, calculation of F/n upon varying one angular variable at a time while keeping the other parameters constant reveals that F/n doubles from the minimal value upon changing β by $\sim 1°$. However, variation of $\pm 10°$ in either α or $\kappa \sim \alpha + \gamma$ are needed to produce the same increase in F/n over the minimum value. Hence, the tilt of the z-axis (β) is considerably more accurately defined in any of the least-square searches for $\mathbf{R}(\alpha,\beta,\gamma)$ than the rhombic axes, ($\kappa \sim \alpha + \gamma$) or the direction of tilt (α). This is confirmed in the three parameter searches for WT metMbCN (Table II), using $\Delta\chi_{ax}$(A) and $\Delta\chi_{rh}$(A), from which variable input data sets yield highly clustered orientations with total ranges of 5° for α, 0.5° for β, and 4° for κ. Similarly clustered values are observed for the two mutants (Table IV). Therefore, we conclude that the present NMR method can determine the orientation of the magnetic axes to within 2° in tilt of the z-axis (β), to $\pm 10°$ in the projection of the tilt on the plane (α), and to within $\pm 10°$ in the projection of the rhombic axes on the heme plane (κ). Moreover, this surprising level of accuracy can be obtained from the minimal data sets (F in Table I) of five δ_{dip} for the strongly shifted, strongly relaxed and resolved resonances.

There are three significant points to the magnetic axes determination for both WT and mutant metMbCN on the basis of the five point minimal data input set F. First, the resulting orientation of the axes in each of the three cases (WT and the two mutants) is extraordinarily close to the orientation determined with the largest data set. Second, the assignments for the required five resonances can be effected solely on the basis of a T_1 measurements[5,33,40] and a pair of 1D NOE experiments[33,40] which can be executed on as little as 2 mg of metMbCN. Hence limited sample size will not preclude determination of the magnetic axes. Last, the magnetic axes resulting from the five parameter fit of the easiest to assign resonances are so close to the true axes that the predictions of δ_{dip} for as yet unassigned resonances provide valuable guidance toward effecting more complete assignments of active site residues. This predictive power is illustrated in Figure 8B, in the plot of δ_{dip}(obsd) versus δ_{dip}(calcd) for all 37 assigned resonances of WT metMbCN based on the $\mathbf{R}(\alpha,\beta,\gamma)$ and $\Delta\chi$ determined solely from five input data points (set F). The δ_{dip} for the 14 resonances not used in the fit are similarly well predicted by the magnetic axes using only the five data point input set F for the E7 Gly metMbCN mutant[41] (Figure 8D). The scatter of points in the plot of δ_{dip}(obsd) for both WT and E7 Gly metMbCN based on magnetic axes determined from only five (data set F) input data points (Figure 8B, 8D) is not significantly greater than when based on the magnetic axes using as input the optimal proximal (14 input data set D) data set (Figure 8A,C). Moreover, in no case do points fall into the upper left and lower right quadrants of Figure 8, indicating that the signs of all δ_{dip} are correctly predicted, i.e., the nodal surface of the dipolar field is very well defined by any of the fits. This is in contrast to the magnetic axes determined for metMbCN based on analysis of ^{1}H and ^{13}C methyl contact shifts,[42] where the resulting axes led not only to a larger scatter in a plot of δ_{dip}(calcd) versus δ_{dip}(obsd) but also to δ_{dip} with incorrectly predicted signs. Insufficient data has been provided in that study to allow a quantitative comparison of the difference in the proposed orientation of the axes.

The determination of the magnetic axes for the distal point mutants makes the explicit assumption that the proximal side of the heme pocket is inconsequentially perturbed by the distal point mutation so that both the crystal coordinates and δ_{dia} for the WT protein may be used. No assumptions are made as to the nature of distal perturbations. The validity of the assumption is supported by numerous crystal studies on WT Mbs significantly perturbed on the distal side by variable ligation states.[11,22,35] The observation of NOESY cross peak patterns in the distal point mutant metMbCN complexes of interest that are unaltered from WT metMbCN[5] both among residues and between residues and the heme *on the proximal side*, as well as conserved paramagnetic-induced relaxation effects, provides direct evidence that this assumption is reasonable. Moreover, X-ray crystal diffraction studies of E7 Gly unligated metMb and MbCO support a conserved proximal side as compared to WT derivatives.[36] Additional confirmation for this assumption is provided by the observation of essentially unaltered δ_{dia} as compared to WT MbCO for the *proximal side residues* in E7 Gly MbCO.[43] The substitution of the available E7 Gly MbCO proximal δ_{dia} for those in the WT MbCO does not have an observable effect on the magnetic axes. Hence the proximal δ_{dia} for the mutants need not be available to determine magnetic axes on a distal point mutant. The strength of the present method is that the magnetic axes of a distal point mutant can be determined solely with δ_{dia} and crystal coordinates of the WT protein.

Since there is not a significant difference in either the orientation of the axes of the error function when the limited distal residues, Phe CD1 and E helix C_αHs, are included (sets B', C'') in the analysis of E7 Gly metMbCN (Table IV), we consider the proximal data set D' (14 points) necessary and sufficient for determination of the magnetic axes in a distal point mutant. An excellent correlation of δ_{dip}(obsd) versus δ_{obs}(calcd) for the proximal data set D' for E7 Gly metMbCN is obtained (Figure 8C). There is some preliminary evidence that the E helix may have moved somewhat, as evidenced by the fact that the backbone E11 C_αH yields an NOE only to 1-CH_3 and not to 8-CH_3 in the E7 Gly mutant, while the same proton gave NOEs to both heme methyls in WT metMbCN. An investigation into the prospect for determining the orientations of perturbed distal residues using the magnetic axes obtained on the basis of unperturbed proximal residues is under investigation on this and other related distal mutants. The least-square searches for WT and E7 Gly metMbCN for a given input data set differ by $\sim 2°$ in β and $\sim 10°$ in κ. The uncertainty of either determination precludes attributing significance to these changes. Hence the tilt of the z-axis and the rhombic axes are largely unaffected; the latter point is consistent with the largely unchanged heme methyl shift pattern which is dominated by contact shifts that reflect the rhombic axes.[2] The orientation of the tilt of the z-axis (α), however, is changed by $\sim 45°$, well outside the uncertainties of either determination. This change clearly reflects a major structural perturbation whose influence on the magnetic axes essentially quantitatively accounts for the strongly perturbed NMR spectrum.

For the CD3 → Gly metMbCN complex, the proximity of Phe CD1 to the point of substitution makes the omission of Phe CD1

(39) Chiu, M. L. Ph.D. Dissertation, University of Illinois, Urbana, 1992.
(40) Ramaprasad, S.; Johnson, R. D.; La Mar, G. N. *J. Am. Chem. Soc.* **1984**, *106*, 5330–5335.
(41) The predicted δ_{dip} for the five signals not assigned for the distal mutants that were utilized in the WT metMbCN magnetic axes determination identify logical candidates for these signals. However, these signals resonate in the crowded aliphatic region and definitive confirmation of their origins via COSY was not possible, and hence the tentative assignments are not listed.
(42) Yamamoto, Y.; Nanai, N.; Chujo, R. *J. Chem. Soc., Chem. Commun.* **1990**, 1556–1557.
(43) Pochapsky, T. C.; Wright, P. E. To be published.

as the source of input data obligatory. In fact, omission of these points does lead to an improvement in the error function (data set C′ → D′ in Table IV). The least-square search using $\Delta\chi_{ax}$(A) and $\Delta\chi_{rh}$(A) for a given data set from CD3 Gly and WT metMbCN leads to differences in α, β, and κ of ~2°, ~0°, and ~5°. With the uncertainties in each determination, the orientation of the axes in the two proteins are undistinguishable based on the searches. It is noted, however, that for each data set, the value for α is more positive by ~2° in CD3 Gly than in WT metMbCN (see below).

The present results bode well for the determination of magnetic axes and magnetic anisotropies for any low-spin ferric WT hemoprotein of diverse function or genetic origin if the X-ray coordinates are available and 2D NMR methods yield the assignments of even a small fraction of the proton signals close to the heme. The needed assignments appear to be attainable not only in the small cytochromes[6] and cyanomet myoglobins,[14] but also in cyanide inhibited heme peroxidases[44] and tetrameric cyanomet hemoglobins.[45] The corollary to this conclusion is that it should be possible to determine the magnetic axes of point mutants (or natural genetic variants) of a reference protein based on the geometric factors for the portion of the protein unperturbed by the substitution(s). Preliminary inspection of the distribution of shifts of as yet unassigned metMbCN spectra of numerous single and double point mutants of metMbCN suggests that it will indeed be possible to develop an interpretive basis of the strongly perturbed shifts based primarily on change in the orientation of magnetic axes.

Utility of Simulations. Since the different restricted input data sets lead to a small range in the orientation (1.0° in β, 10° in α, and 10° in κ) as discussed in detail above, it is also obvious that a least-square search that yields the orientation of axes for a mutant that differs from that of the reference protein by <1.0° in β, <10° in α, and <10° in κ may or may not be significant. The simulations in Figure 7, however, have the prospect for potentially identifying the precise nature of small changes in the orientation of magnetic axes where a least-square search on a mutant yields very similar $\mathbf{R}(\alpha,\beta,\gamma)$. A case in point is the CD3 Gly metMbCN complex, for which the magnetic axes indicate tilt and projection smaller than the range in angles for variable input data for WT. Upon analysis of the shift difference between WT and CD3 Gly met MbCN for the proximal residues (set D′) whose orientations are unlikely to change upon the CD3 substitution on the distal side (Table III), we find that the His F8(93) ring $C_\delta H$ and $C_\epsilon H$ and Ile FG5(99) dipolar shifts are all larger in the mutant and can be explained as an increase in either α or β.[46,47] However, the key His FG3(93) $C_\delta H$ and His F8 $C_\beta H$ signals exhibit dipolar shift changes (Figure 7) that support the conclusion that the major difference between WT and CD3 Gly metMbCN is a small change in α rather than in β, and that the change in α is to a more positive value. The magnitudes of the observed shift changes in Table III, when compared to the slopes of the lines in Figure 3, indicate that α has become more positive by ~2°.

While the His F8 ring CH hyperfine shifts do not provide a unique probe of the tilt of the magnetic axes,[5] observed changes in these shifts provide important confirmation of the validity of the magnetic axes and anisotropies determined from a least-square search. Thus the calculations of the His F8 contact shifts yield a pattern that is the same for either the WT or E7 Gly metMbCN, as well as for the model compound outside the protein matrix (see the supplementary material). Moreover, the *differences between WT and E7 Gly metMbCN in the calculated δ_{dip} for the His F8 $C_\delta H$, $C_\epsilon H$, and $C_\beta H$ are* +15.4, −16.1, and +2.5 ppm, which are remarkably close to the observed shift difference[43] for the same proteins, +15.2, −14.3 ± 2.5, and +1.5 ppm, respectively. Thus the altered His F8 hyperfine shifts are essentially quantitatively accounted for by the calculated difference in the magnetic axes. While the His F8 shifts play no direct role in determining magnetic axes, the observed shift pattern for His F8 provides a valuable quantitative confirmation of the altered magnetic axes.

The determination of the magnetic axes for the E7 Gly mutant indicates that the degree of tilt is essentially unchanged from that of the WT, but that the direction of the tilt is changed by a ~45° clockwise rotation in Figure 1A. On the basis of the reasonable supposition that the tilted magnetic z-axis is directly related to tilt of the Fe–CN unit, this suggests that the E7 His sidechain is not the major determinant of the ligand tilt. However, such a conclusion is in contrast to the classical text book picture[19] of the origin of sterically induced distal ligand tilt in Mbs. A more detailed interpretation of the structural bases of the altered magnetic axes is deferred until such studies can be extended to test the generality of the response to the magnetic axes to E7 substitution.

Acknowledgment. The authors are indebted to Dr. S. D. Emerson for providing the computer program used in this study and to A. McPherson for assistance with the use of the programs. This research was supported by grants from the National Institutes of Health, HL 16087 (G.N.L.) and GM-33775 (S.G.S).

Registry No. His, 71-00-1; Arg, 74-79-3; Gly, 56-40-6.

Supplementary Material Available: Five tables (heme chemical shifts for WT, E7 Gly, CD3 Gly metMbCN, orientation of magnetic axes using theoretical anisotropies, chemical shift analysis of amino acids in E7 Gly and CD3 Gly metMbCN mutants, separation of His F8 hyperfine shifts net dipolar and contact contribution) and four figures (magnitude COSY, NOESY (2) map for CD3 Gly mutant metMbCN, and plot of observed dipolar shift versus variable temperature slopes for amino acid signals of E7 Gly metMbCN mutant) (9 pages). Ordering information is given on any current masthead page.

(44) de Ropp, J. S.; La Mar, G. N. *J. Biomolec. NMR* **1991**, *1*, 175–190.
(45) Sylvia, A.; La Mar, G. N. Unpublished data.
(46) The δ_{obsd} in WT metMbCN minus the δ_{obsd} from E7 Gly metMbCN, as given in Table III.
(47) The Phe CD1(43) $C_\zeta H$ shift is essentially unchanged. However, proximity of the CD3 substitution to Phe CD1 on the CD corner suggests that it is unreasonable to assume that the Phe CD1 orientation is completely unperturbed and hence does not serve as a test for the simulation studies.